Reprint from

Rarefied Gas Dynamics

Edited by Alfred E. Beylich

VCH Weinheim · New York · Basel · Cambridge

Brownian-Motion Limited Aerodynamic Focusing of Heavy Molecules

R. Fernández-Feria,[b] P. Riesco-Chueca,[b] J. Rosell-Llompart,[a] J. O'Brien,[a] and J. Fernández de la Mora [a,*]
[a] Yale University, P.O. Box 2159 Y.S., New Haven, CT 06520, USA
[b] E.T.S.I.I., Av. Reina Mercedes s/n. 41012 Sevilla, Spain

Thermal agitation is the major phenomenon limiting how narrowly a beam of heavy molecules suspended in a light carrier gas can be focused by acceleration through a converging nozzle. Here, the problem is studied numerically by two different methods: hypersonic theory and Brownian dynamics simulation, with a good agreement between both. A near-axis simplification of the hypersonic equations yields the focusing characteristics of inviscid two-dimensional flows in nozzles with straight walls converging at various angles.

I. INTRODUCTION

A recent extension of earlier experimental and theoretical work[1,2] has shown the possibility of sharply focusing microscopic particles suspended in a carrier gas practically into a point, by acceleration through a converging nozzle.[3,4] Evidently, this kind of aerodynamic focusing would be of considerable interest if it could also be attained in the case of heavy molecules suspended in a light gas (He or H_2). Unfortunately, the minimum width d_m of the focused beam appears to be seriously limited by the thermal motion of the heavy particles.

An order of magnitude analysis[3] shows that, for sonic nozzles, d_m is of the order of $(m/m_p)^{1/2}$ times the diameter d_n of the accelerating nozzle, where m and m_p are the molecular masses of the carrier and heavy gases, respectively. However, experimental work with mixtures where $m_p/m \sim 160$ has shown that such an estimate underpredicts the minimal focal width by a factor typically larger than five, so that d_m/d_n is as large as 0.4 (rather than 0.075), even for the extreme case of $H_2 - W(CO)_6$ mixtures.[5] Such a modest geometrical concentration would preclude any truly singular manifestation of the focusing phenomenon for all conceivable molecules with non-negligible volatility, unless design conditions far more favourable than those of reference 5 could be found. In this article we extend earlier work[3] in order to compute the effect of Brownian motion on the minimum width of a beam of heavy molecules which would otherwise be infinitely narrow. Hopefully, the numerical techniques developed will guide the design of optimal focusing nozzles capable of minimizing Brownian focal broadening.

The Brownian movement in gas mixtures far from equilibrium cannot be described by the standard fluid dynamical equations. Accordingly, because under conditions leading to aerodynamic focusing the heavy gas is strongly uncoupled from the carrier, its theoretical description requires a kinetic theory. Although under the present circunstances characterized by a large mass disparity ($m_p/m \gg 1$) one may use the Fokker-Planck[6] rather than the Boltzmann equation, still, this reduced kinetic equation in 6 dimensional phase space is most often numerically intractable as a partial differential equation. It can however be attacked via Brownian dynamic (B.D.) simulations.[7,8,9] Alternatively, a simplification arises for the case of a focusing beam, due to the fact that the ratio of convective to thermal speed of the heavy gas [a Mach number which, when the light gas jet is sonic, takes values of order $(m_p/m)^{1/2}$] is a large number. One may then systematically close the problem at a hydrodynamic level by means of a hypersonic theory (H.T.) which retains the effect of thermal agitation.[10,11] The accuracy of this hypersonic closure has been succesfully tested against some exact solutions to the Fokker-Planck equation.[10,11] Furthermore, the hyperbolic nature of the hypersonic equations within their range of validity permits a relatively easy numerical attack for complex flows by the method of characteristics

(M.C.). The accuracy and convenience of this numerical method has also been established by comparison with existing solutions to the Fokker-Planck equation.[12]

In the next section we introduce the H.T. and solve the equations by the M.C. A near-axis simplification of the H.T. is succesfully tested against these results, and used then to characterize the focal region. A comparison of the hypersonic results with B.D. simulations is made in Section III, which is followed by a discussion and a comparison with experiments.

II. HYPERSONIC THEORY

II.1 Governing Equations. The following theoretical study is based on the lowest order hypersonic closure of the hydrodynamic equations for the heavy gas, which incorporates Brownian motion effects. In this approximation, the pressure tensor P_p is preserved in the momentum equation, and the heat flux is neglected in the conservation equation for P_p :[10-13]

$$D\lambda_p = -\nabla \cdot \mathbf{U}_p \quad , \quad D\,\mathbf{U}_p + \epsilon^2[(T_p \cdot \nabla)\lambda_p + \nabla \cdot T_p] = (\mathbf{U} - \mathbf{U}_p)/S \ ,$$

$$D\,T_p + (T_p \cdot \nabla)\mathbf{U}_p + [(T_p \cdot \nabla)\mathbf{U}_p]^T = 2(T\,I - T_p)/S \ , \quad (D \equiv \partial/\partial t + \mathbf{U}_p \cdot \nabla) \ . \qquad (1)$$

In these equations, $\lambda_p = \log(\rho_p/\rho_{po})$, where ρ_p is the heavy species density and ρ_{po} a reference density; $\mathbf{U}_p$ and $T_p \equiv P_p m_p/k\rho_p$ are, respectively, the dimensionless heavy gas velocity and temperature tensor; $\mathbf{U}$ and $\mathbf{T}$ are the carrier gas velocity and temperature; the dimensionless parameters S (Stokes number, which measures the decoupling between both species) and ϵ (inverse of the heavy gas Mach number) are defined by

$$S = U_R\,\tau\,/\,L_R \quad , \quad \epsilon^2 = k\,T_R\,/\,m_p\,U_R^2 << 1 \quad , \qquad (2)$$

where L_R, U_R and T_R are a reference length, velocity and temperature, k is Boltzmann's constant, and τ is the heavy gas relaxation time, related to its diffusivity D in the carrier gas through Einstein's law $D = kT\tau\,/m_p$.

The computations in this section correspond to the two-dimensional geometry of Fig.1, with semiangles $\theta = 90^\circ, 60^\circ, 45^\circ$ and 30°, which, when $\mathbf{U}$ is given by potential flow theory and T is constant, constitutes an efficient aerodynamic lens.[4] We take $T_R = T$, $U_R = Max[mod(\mathbf{U})]$ and $L_R = d_n/2$.

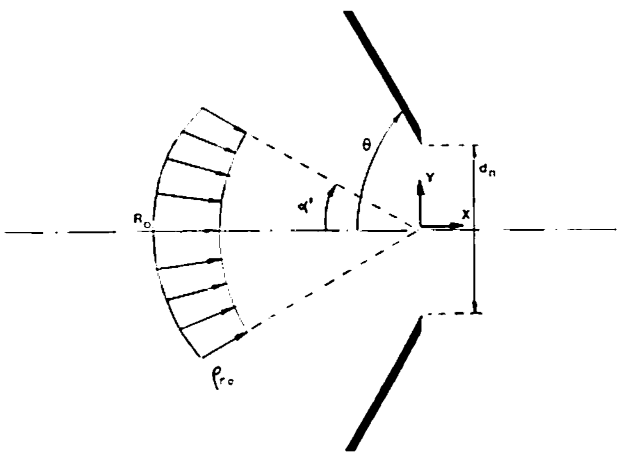

Fig. 1 Seeding conditions for heavy molecules injected in an inviscid incompresible gas.

II.2 Integration by the method of characteristics. For this case we consider only a nozzle angle $\theta = 90^o$. The heavy species is seeded far upstream with uniform density on an arc of angle α' (see Fig. 1), and Eqs. (1) are solved via the M.C.[12] Since the seeding arc is relatively close to the orifice ($R_o = 2\,L_R$), the initial value of the heavy gas velocity departs from that of the carrier gas; assuming far upstream equilibrium conditions, the velocity at R_o can be approximated through $\mathbf{U}_p \simeq \mathbf{U} - S(\mathbf{U}\cdot\nabla)\mathbf{U}$. In the case of $S = 3$, which is the highest Stokes number that has been used here, the correction is about 30%. and the corresponding error is of the order of its square. The initial temperature tensor is taken to be $T_p = T\,I$. This quantity departs also from the value corresponding to equilibrium far upstream by a quantity of order $S(T_p\cdot\nabla)\mathbf{U}_p$. The corresponding correction, however, is anisotropic and complicates considerably the initiation of the integration process. Accordingly, although these results do not correspond strictly to equilibrium initial conditions, they embody a complete solution to the H.T. with which other approximate results can be compared. For the numerical computations, a grid of vertical lines is used, with a separation of $\Delta x = 0.001$. The M.C. is started at the first of these vertical lines (x_o) where the properties are evaluated from the initial conditions at the seeding arc in the following fashion: The points in $x = x_o$ swept by the Prandtl-Meyer fan emerging from the corner of the seeding arc are characterized using the exact solution given in Ref. 12, Sec. III.B, while the position and properties of the remaining interior points are obtained from a deterministic integration along the trajectories. Once the heavy component properties at x_o are known, the M.C. is followed to evaluate them at succesive lines x_1, x_2, ..., until the focal region is passed. The numerical computations take more than half an hour of CPU time for each run, because one has to solve seven ordinary differential equations along five different characteristic directions for each grid point (see Ref.12 for the details of the method). Typical density profiles of the heavy component are shown in Fig. 2 for $\epsilon = 0.05$, $S = 3$ and $\alpha' = 20^o, 45^o$. Notice that the beam width (measured by the coordinate $y_{1/2}(x)$ such that $n[y_{1/2}, x] = n(0, x)/2$) reaches a minimum at a *focus* near $x = 1.2$. Furthermore, $y_{1/2}$ is independent of the seeding angle α' (Fig.3), and is nearly linear with ϵ.

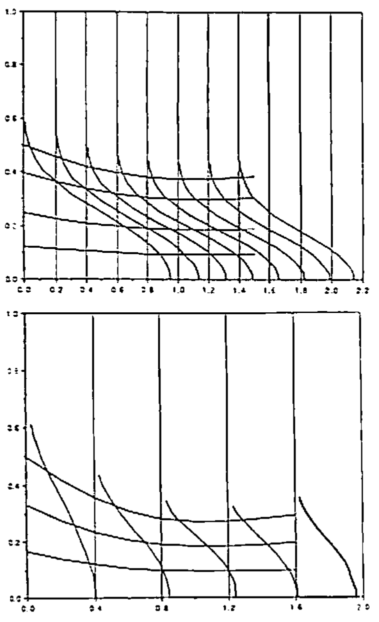

Fig. 2: $a-b$ Transversal density profiles and trajectories from the method of characteristics for $S = 3$, $\epsilon = 0.05$ and $\alpha' = 20^\circ$ (in a) and $\alpha' = 45^o$ (in b).

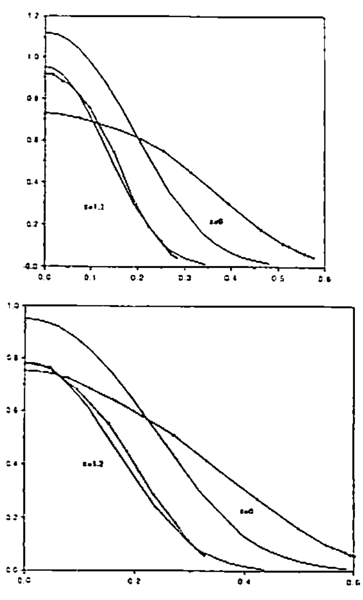

Fig. 3: $a-b$ Transversal density profiles at the nozzle exit ($x = 0$) and at the focal point for $\epsilon = 0.05$, $\alpha' = 20^\circ$, 45°, and $S = 3$ (in a) and $S = 2$ (in b). The marked curves correspond to $\alpha' = 45^\circ$.

II.3 Near-axis theory for a Gaussian density profile. The structure of the focal region can be more easily studied with a simplification of Eqs. (1) valid near $y = 0$, where one keeps only lower order terms in an expansion in powers of y. Defining the new transversal coordinate $\eta \equiv y/\epsilon$, of order unity near the axis, and taking the radial particle velocity and density profiles to be linear, and Gaussian in η, respectively, the problem admits a solution with the following structure: $\lambda_p \equiv \lambda_o(x) + \eta^2 \lambda_1(x)$, $U_{px} \equiv u_o(x) + \epsilon^2 u_1(x,\eta)$, $u_1 = p(x) + \eta^2 q(x)$, $w \equiv U_{py}/\epsilon = \eta\, w_o(x)$, $T_{pxx} \equiv T_1(x)+\epsilon^2 T_{11}(x,\eta)$, $T_{pyy} \equiv T_2(x)+\epsilon^2 T_{21}(x,\eta)$, $T_{pzz} \equiv T_3(x)+\epsilon^2 T_{31}(x,\eta)$, $\theta_{xy} \equiv T_{pxy}/\epsilon = \eta\, \beta(x)$. In terms of the light gas quantities $U_x \equiv u_{lo}+\epsilon^2 \eta^2 u_{l1}(x)$, $U_y \equiv \epsilon\, \eta\, w_{ol}(x)$, $T_l \equiv T_{lo}(x) + \epsilon^2 \eta^2 T_{l1}(x)$, up to second orden in ϵ Eqs. (1) become[3,13]

$$u_o \frac{d\lambda_o}{dx} + \frac{du_o}{dx} + w_o(1+\phi) = 0\,, \quad u_o \frac{d\lambda_1}{dx} + 2\, w_o \lambda_1 = 0\,, \quad u_o \frac{du_o}{dx} + \frac{u_o - u_{lo}}{S} = 0\,,$$

$$u_o \frac{dw_o}{dx} + w_o^2 + \frac{w_o - w_{lo}}{S} + 2\, T_2 \lambda_1 = 0\,, \quad u_o \frac{dT_1}{dx} + 2\, T_1 \frac{du_o}{dx} + 2\, \frac{T_1 - T_{lo}}{S} = 0\,,$$

$$u_o \frac{dT_2}{dx} + 2\, T_2\, w_o + 2\, \frac{T_2 - T_{lo}}{S} = 0\,, \quad u_o \frac{dT_3}{dx} + 2\, \phi\, T_3\, w_o + 2\, \frac{T_3 - T_{lo}}{S} = 0\,,$$

$$u_o \frac{d\beta}{dx} + \beta \left(\frac{2}{S} + 2\, w_o + \frac{du_o}{dx} \right) + 2\, T_2\, q + T_1 \frac{dw_o}{dx} = 0 \quad ,$$

$$u_o \frac{dp}{dx} + p \frac{du_o}{dx} + T_1 \frac{d\lambda_o}{dx} + \frac{dT_1}{dx} + \beta(1+\phi) + \frac{p}{S} = 0 \quad ,$$

$$u_o \frac{dq}{dx} + 2\, w_o\, q + q \frac{du_o}{dx} + T_1 \frac{d\lambda_1}{dx} + 2\, \beta\, \lambda_1 + \frac{q - u_{l1}}{S} = 0 \quad ,$$

where $\phi = 0, 1$ for two-dimensional and axisymmetric flows, respectively. To check how general these near-axis equations are, we have solved them starting at $x = 0$ (nozzle exit) with the results from the M.C., approximating the density at $x = 0$ by a Gaussian profile. Fig. 4 shows the axial profiles of density ($\exp(\lambda_o)$), axial and transversal velocity and temperature as obtained from the M.C. and from the near-axis equations (u_o, w_o, T_1 and T_2). Also included is the profile of heavy component jet width $y_{1/2}$. The value of ϵ is 0.05, S is 2 or 3, and α' is 20 or 45 degrees. A few observations can be made from these figures. As noted before, the particle jet width reaches a minimum, corresponding to the focal region. Somewhere around this point, the transversal temperature T_2 reaches a maximum, and the transversal velocity gradient w_o goes through zero (from negative in the pre-focal region, where inertia and drag prevail to determine a converging heavy molecules flow, to positive in the post-focal region, where heavy molecules either cross the axis or start being dominated by Brownian diffusion). The axial velocity and temperature, u_o and T_1, have monotonous trends in their relaxation towards the background properties. They are very accurately described by the near-axis solution, which happens to be the same as in a deterministic formulation.[4] The other variables (density, jet width and transversal temperature, related to λ_o, λ_1 and T_2 in the near-axis model) are fairly well predicted by the near-axis analysis when $\alpha' = 20^\circ$, showing, however, important differences when $\alpha' = 45^\circ$, when they overestimate T_2 and λ_1 with respect to the M.C. (indeed, when the seeding angle is wide, the assumptions made in the near-axis equations are far from being accurate). Ref.3 reports an analytical description of the focal structure which predicts that the minimal beam width is independent of the seeding angle, in agreement with the results from the M.C.

II.3.1 Focal characteristics for varying nozzle angles θ. The results of the previous section show that the near-axis simplification of the H.T. is accurately consistent with the full hypersonic equations when the seeding angle is not very wide. In practice, it is desirable to seed the particles only in the axial region of the jet in order to eliminate defocusing due to geometric aberration.[4] For this reason we use these *paraxial* equations to characterize the size and location of the focal region as a function of the parameters that govern the problem. Table I gives the jet width $\eta_{1/2,m} = y_{1/2,m}/\epsilon$ at the focal point for some values of ϵ, the Stokes number

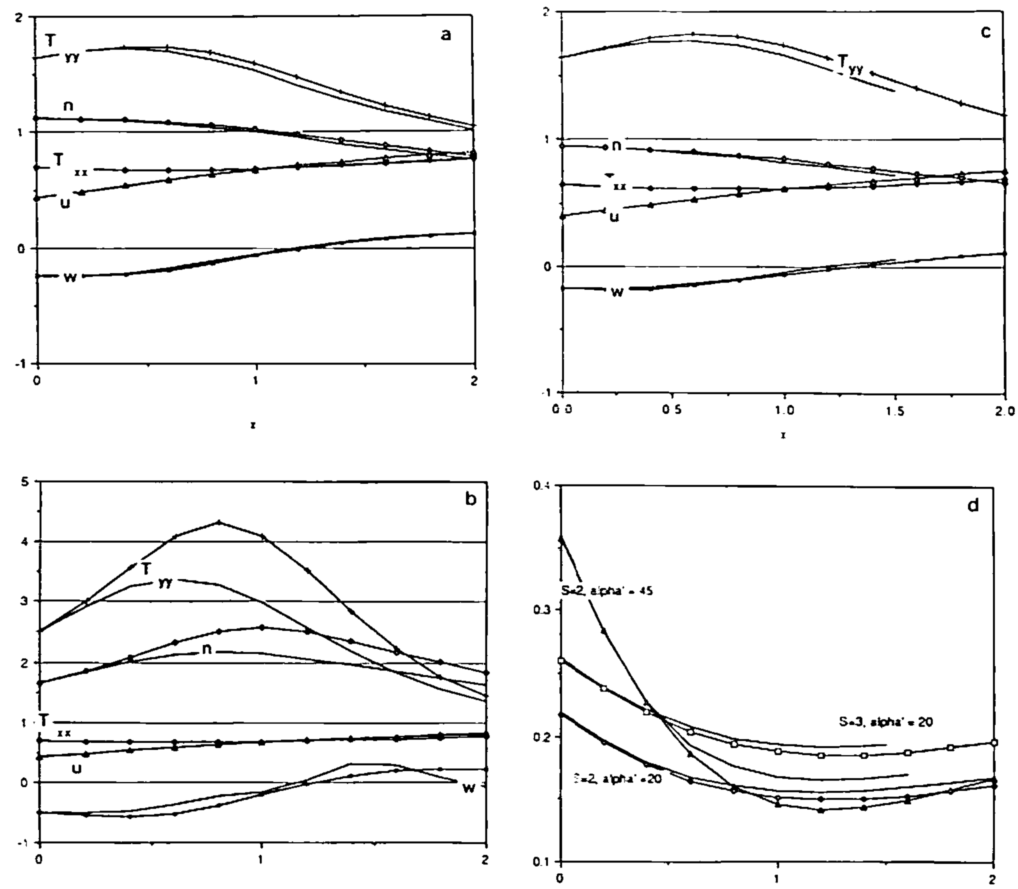

Fig. 4: $a - d$ Density profiles (n), axial and transversal temperatures (T_{xx} and T_{yy}), axial velocity (u) and transversal velocity gradient (w) along the axis as obtained from the method of characteristics and from the near-axis hypersonic equations (marked curves). Figures a to c correspond to ($S = 2$, $\alpha' = 20^\circ$), ($S = 2$, $\alpha' = 45^\circ$) and ($S = 3$, $\alpha' = 20^\circ$), respectively. $\epsilon = 0.05$ for all curves. Also included (Fig. 4-d) is the jet width $y_{1/2}$ as a function of x for the three cases.

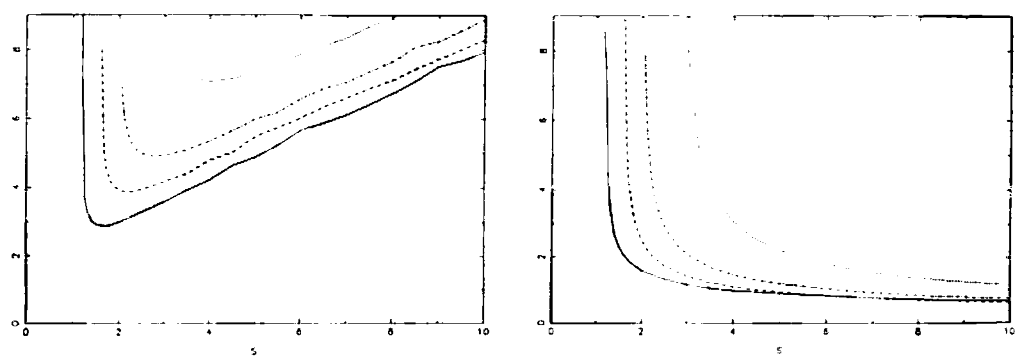

Fig. 5: $a - b$ Minimum of the jet width $\eta_{1/2m}$, and focal distance x_f as a functions of the Stokes number S for $\theta = 90^\circ$ (continous line), 60° (dashed line), 45° (dashed and dotted line), and 30° (dotted line).

S, the nozzle angle θ, and the initial jet width at $x = -5$, $y_{1/2,o}$. As shown before, the minimum jet width, $\eta_{1/2,m}$, depends neither on ϵ nor on the seeding jet width $y_{1/2,o}$, and it ranges, in the cases here computed, between 3.5 and 6, increasing with θ. The focal distance x_f is also almost independent of ϵ and $y_{1/2,o}$, increasing when either θ or S decrease.

S	θ	$y_{1/2,o}(x=-5)$	ϵ	$\eta_{1/2m}$	x_f	S	θ	$y_{1/2,o}(x=-5)$	ϵ	$\eta_{1/2m}$	x_f
3	90	2	0.001	3.56	1.16	5	90	2	0.001	4.85	0.88
3	90	2	0.01	3.56	1.16	5	90	2	0.01	4.84	0.91
3	90	4	0.001	3.58	1.16	5	90	4	0.001	4.85	0.88
3	90	4	0.01	3.56	1.16	5	90	4	0.01	4.85	0.89
3	60	2	0.001	4.13	1.41	5	60	2	0.001	5.32	0.93
3	60	2	0.01	4.13	1.39	5	60	2	0.01	5.30	0.94
3	60	4	0.001	4.17	1.40	5	60	4	0.001	5.45	0.93
3	60	4	0.01	4.13	1.40	5	60	4	0.01	5.31	0.93
3	45	2	0.001	4.92	2.08	5	45	2	0.001	5.89	1.19
3	45	2	0.01	4.90	2.01	5	45	2	0.01	5.88	1.18
3	45	4	0.001	4.91	2.09	5	45	4	0.001	5.97	1.19
3	45	4	0.01	4.92	2.07	5	45	4	0.01	5.88	1.19

Table I. Width and location of the focal region for some values of S, θ, ϵ and seeding width $y_{1/2,o}$.

Figure 5 shows the influence of S on $\eta_{1/2,m}$ and x_f for nozzle angles $\theta = 90, 60, 45$ and 30 degrees. It is seen that, as S increases, the focal jet width $\eta_{1/2,m}$ decreases very rapidly untill it reaches a minimum for a certain value of $S = S^*$ (which depends on θ). The focal distance x_f decreases monotonically as S increases: first very rapidly, until $S \simeq S^*$, and then slowly. On the other hand, as θ decreases, both x_f and $\eta_{1/2,m}$ increase. Thus , a nozzle angle of 90° is the most efficient in concentrating heavy molecules, yielding a minimum of the jet width as low as $\eta_{1/2,m} \simeq 2.85$ (i.e., d_m/d_n about $2.85(m/m_p)^{1/2}$) for $S^*(90^o) \simeq 1.6$, at $x_f \simeq 2.05$. (Notice that the deterministic computations of Ref.3, Sec.V.D. use half of the width of the carrier gas jet far downstream, b, as the reference length L_R, instead of $d_n/2$ used here.)

III. COMPARISON WITH BROWNIAN DYNAMICS SIMULATIONS

In order to further assess the precision of the H.T., we have carried out simulations using the technique of B.D.,[7,8] modified more recently[9] to allow the computation of spatial variations of particle-phase properties. Brownian dynamics, as applied here, produces essentially exact solutions of the Fokker-Planck equation by simulating large numbers of particle trajectories. To further simplify the simulations, we employed as a model flow field the potential flow through a two-dimensional hyperbolic nozzle, which may be written in complex notation as $U_x - iU_y = -1/\sqrt{1+z^2}$, where z represents position through $z = x + iy$. Each of our simulation runs was carried out using a Stokes number, $S = 4$, large enough for a focal point to exist. Particle properties were collected at about 40 axial locations or *tripwires*, with 16 radial bins or sampling points at each tripwire (the radial extent of sampling at a given tripwire was determined by performing a short run first and observing the maximum radial position attained by a particle). The time step was dynamically adjusted according to the local carrier gas velocity gradient, allowing the simulation to proceed quickly in regions where the particles are not too far from equilibrium with the host fluid.

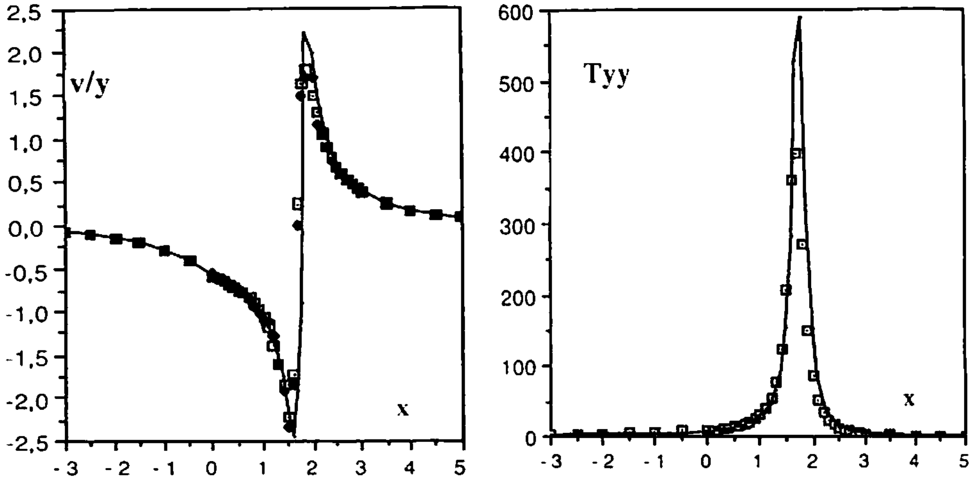

Figure 6: Comparison between B.D simulations (symbols) and H.T (continuous lines).

Figures 6 present comparisons between the B.D. results (symbols) and the H.T. (lines). In each case, the initial conditions for the numerical integration of the hypersonic results were taken to be the same as those from the simulation point furthest upstream. The beam widths (not shown) agreed very well, with some 10% discrepancy past the focus. On the left we show w=v/y on the axis, with fairly good overall agreement. On the right one can see T_{yy} along the axis, showing nearly 50% disagreement at the peak, although the shape of the profile is well represented. We do not know still which of the two computational procedures is most responsible for the disagreement

IV. COMPARISON WITH EXPERIMENTS

Here we report measured values of $y_{1/2}$ as a function of ϵ, for hypersonic seeded jets expanding through round thin-plate orifice nozzles. The heavy species used were $W(CO)_6$, CBr_4, C_2Cl_6, CCl_4, and Ar, with m_p ranging between 352 and 40. The experimental system has been described in Ref.5. These viscous thre-dimensional compressible flows are quite different from those considered in earlier sections. Nonetheless, the focusing role of inertia and the broadening effect of Brownian motion are identical in both cases. Using for T_R and U_R the source stagnation temperature and the carrier gas sound speed, then $\epsilon^2 = \gamma m/m_p$, where $\gamma = 1.4$ and $5/3$ for H_2 and He, respectively. The beam widths $d^* = 2y_{1/2}$ reported (all lenghts are made dimensionless through the nozzle orifice diameter d_m) depend on m/m_p, S, and on the axial distance x to the nozzle. Rather than its absolute minimum for each mass ratio, we have minimized it sweeping over S for fixed values of $x = 1.3$ and 3.2. When plotting d^* vs. $(m/m_p)^{1/2}$, the curves are reasonably linear over the range of masses explored, and can be fitted by the expressions $d^* = \alpha + \beta(m/m_p)^{1/2}$, with the values of $\alpha = 0.193, 0.393$, and $\beta = 2.69, 4.162$ for mixtures in H_2 at $x = 1.3$ and 3.2, respectively, and $\alpha = 0.13, 0.096$ and $\beta = 3.29, 7.01$ for He mixtures under identical conditions. The corresponding value of $\eta_{1/2}$ is 3.2 for the most favourable case of very small ϵ in H_2 at $x = 1.3$. This number does not differ much from the most favourable one found numerically out of all geometries and hydrodynamical conditions explored. Because it is not very likely that substantially better design conditions might be found, a sad conclusion results: It does not appear to be possible to concentrate aerodynamically any volatile heavy vapor within a diameter 10 times smaller than the diameter of the accelerating nozzle. High resolution aerodynamic focusing belongs exclusively to situations with mass ratios of tens of thousands, attainable only with microscopic particles several nanometers in diameter or with macromolecules.

ACKNOWLEDGEMENTS

This work has been supported by the US Department of Energy Grant DE-FG02-87ER13750, by the National Science Foundation Grants CBT-8812070 and CBT-8809548, and by the Department of Defense ARO contract GAAL 03-87-K-0127D at Yale.

REFERENCES

1. Israel, G.W. and Friedlander, S.K. "High Speed Beams of Small Particles", J. Coll. Interf. Sci., Vol. **24**, 1967, pp. 330-337.

2. Dahneke, B.E., Hoover, J. and Cheng, Y.S., "Similarity Theory of Aerosol Beams", J. Coll. Interf. Sci., Vol. **87**, 1982, pp. 167-179.

3. Fernández de la Mora, J., Rosell-Llompart, J. and Riesco-Chueca, P., "Aerodynamic Focusing of Particles and Molecules in Seeded Supersonic Jets", Rarefied Gas Dynamics, edited by E.P. Muntz, D.P. Weaver and D.H. Campbell, 1989, pp. 247-277.

4. Fernández de la Mora, J. and Riesco-Chueca, P., "Aerodynamic Focusing of Particles in a Carrier Gas", J. Fluid Mech., Vol. **195**, 1988, pp. 1-21.

5. Fernández de la Mora, J. and Rosell-Llompart, J., "Aerodynamic Focusing of Heavy Molecules in Seeded Supersonic Jets", J. Chem. Phys., Vol. **91**, 1989, pp. 2603-2615.

6. Wang Chang, C. and Uhlenbeck, G.E., in Studies in Statistical Mechanics, Vol. **V**, pp. 89-92, edited by J. De Boer and G.E. Unlenbeck, North Holland, Amsterdam, 1970. Also, Fernández de la Mora, J. and Fernández-Feria, R., "Kinetic Theory of Binary Gas Mixtures with Large Mass Disparity", Phys. Fluids, 1987, Vol. **30**, pp. 740-751.

7. Ermak, D.L. and H. Buckholtz, J. Comp. Phys., **35**, 169, 1980.

8. Gupta, D. and Peters, M.H., J. Colloid Interface Sci., **104**, pp. 375-389, 1985.

9. O'Brien, J.A., J. Colloid Interface Sci., **134**, pp. 497-521, 1990.

10. Fernández-Feria, R., "Hypersonic Expansion of the Fokker-Planck Equations", Phys. Fluids A, 1989, Vol. **1**, pp. 394-402.

11. Riesco-Chueca, P. and Fernández de la Mora, J., "Brownian Motion far from Equilibrium: A Hypersonic Approach", J. Fluid Mech., 1990, Vol. **214**, pp. 639-663.

12. Riesco-Chueca, P., Fernández-Feria, R. and Fernández de la Mora, J. "Method of Characteristics Description of Brownian Motion far from Equilibrium", Rarefied Gas Dynamics, edited by E.P. Muntz, D.P. Weaver and D.H. Campbell, 1989, pp. 311-325.

13. Riesco-Chueca, P., "Non-Equilibrium Dynamics of Binary Gas Mixtures with Large Mass Disparity", Ph. Thesis, 1988, Yale University.

(*) On leave at Dep. Fisica Fundamental, UNED, Madrid, Spain.